

# Low Amplitude Nonlinear Damping and Effective Modulus in Magnesium Alloys Containing Long-Period Stacking Ordered Structures

D.A. Kalganov<sup>1,\*</sup> , S.A. Philippov<sup>1,2</sup> , V.V. Kaminskii<sup>3</sup> , A.Yu. Ivanov<sup>3</sup> ,  
S.V. Zasyplin<sup>4</sup> , D.L. Merson<sup>4</sup> , M.V. Dorogov<sup>3</sup> 

<sup>1</sup> Laboratory of Diffraction Methods for Investigation of Real Crystal-Structures, Ioffe Institute, Politeknicheskaya, 26, St. Petersburg, 194021, Russia

<sup>2</sup> Peter the Great St. Petersburg Polytechnic University, Politeknicheskaya, 29, St. Petersburg, 195251, Russia

<sup>3</sup> Institute of Advanced Data Transfer Systems, ITMO University, Kronverkskiy pr., 49, lit. A, St. Petersburg, 197101, Russia

<sup>4</sup> Institute of Advanced Technologies, Togliatti State University, Belorusskaya, 14, Togliatti, 445020, Russia

---

## Article history

Received March 13, 2025  
Accepted March 28, 2025  
Available online March 31, 2025

## Abstract

In this paper, the microstructure and phase composition of magnesium alloys obtained by casting from a furnace charge mixture of the Mg–2.6Y–1Zn–0.5Gd–0.2Zr–0.1Yb system are characterized. It is found that it contains about 10% of the long-period stacking ordered phase. Low-amplitude nonlinear damping and softening of the elastic modulus are studied using the composite piezoelectric resonator method. The time dependence of elasticity and microplasticity is revealed, which is explained by the redistribution of point defects in the elastic fields of dislocations. It has been established that the activation temperature of this mechanism is 227 K, this is confirmed by the presence of the stress relaxation peak on the temperature dependence of damping, as well as the absence of its time dependence at low-temperature deformation of 163 K.

---

**Keywords:** Anelasticity; Nonlinear damping; Effective modulus; Magnesium alloy, Long-period stacking ordered structure

## 1. INTRODUCTION

Work aimed at improving the engineering properties (strength, crack and corrosion resistance) of magnesium-based materials has been carried out for a long time by many scientific groups [1–3]. However, the number of ways to enhance their performance characteristics is limited. Improving mechanical properties of *hcp*-metals like magnesium through thermomechanical processing and severe plastic deformation is difficult and usually requires elevated temperatures, which leads to recrystallization and reduced treatment efficiency [4]. Modification of magnesium alloys by addition of reinforcing particles requires optimization of uniform distribution and interface bonding of nanoparticles. Production of such composites on an industrial scale is not possible with the current development

of processing technologies, but future engineering advances may allow the production of new materials of this kind [5].

Ternary magnesium alloys, such as Mg–Zn–Al and Mg–Zn–Zr with fine-grained structures are widely used in industrial fields; however, there is still no clear and systematic understanding of the effects of various alloying elements on the properties of magnesium [6]. It is well known that zinc effectively hardens magnesium alloys through solid solution strengthening mechanism and can also control their corrosion properties [7]. Al-bearing magnesium alloys do not have an ideal grain refiner and are processed to modify the microstructure mainly by plastic deformation methods [8]. A specific feature of the Mg–Zr ligature—an additive in the production of magnesium alloys—is the high ability to complicate the grain

---

\* Corresponding author: D.A. Kalganov, e-mail: [d.a.kalganov@mail.ioffe.ru](mailto:d.a.kalganov@mail.ioffe.ru)

structure [9]. Due to the structure conformity an  $\alpha$ -Zr to  $\alpha$ -Mg and high growth restriction factor, the Mg–Zr system provides the possibility to realize ultrafine graining of the material without additional processing. Grain refinement entails precipitation strengthening effect, and other strengthening factors, which enhances the consumer properties of alloys.

During heat treatment of Mg–TM–RE alloys (TM is transition metal and RE is rare earth element), the so-called long period stacking ordered (LPSO) phase is often obtained [10]. In the Mg–Zn–Y systems the LPSO phase consists of a solid solution of Y and Zn in a magnesium matrix, where these atoms are periodically arranged in the basal planes of magnesium to form an ordered structure. Various structures of LPSO have been reported in the literature, i.e., 6H, 10H, 14H, 18R, and 24R, depending on the thermal history of the material [11,12]. The LPSO phase shows good thermodynamic stability at high temperatures, and acting as an effective strengthening phase, LPSO affects the mechanical properties of materials, increasing the plasticity of the material and the strength of the magnesium alloy [13].

Studies of internal friction (IF) using the Marx resonator method [14] make it possible to determine the effective modulus of elasticity in the region of small (up to  $10^{-4}$ ) strain amplitudes, as well as make important assumptions about the nature of anelastic and plastic deformation in metals, alloys and composites [15,16]. In this method, data on anelastic properties of materials are obtained from measurements of the effective modulus  $E$  and elastic vibration damping  $\delta$  at high frequencies  $f \sim 10^5$  Hz and strain amplitudes  $\varepsilon$  up to  $10^{-4}$ . Typically, small amplitudes  $\varepsilon < 10^{-6}$  describe dynamic elastic properties (modulus  $E_i$ ) and amplitude independent damping  $\delta_i$ . With further increase in strain, nonlinear amplitude-dependent damping  $\delta_h = \delta - \delta_i$  and amplitude-dependent softening of the elastic modulus  $\Delta E / E = (E - E_i) / E_i$  occur. Microplastic properties can be represented in standard stress-strain coordinates using values of stress from Hooke's law  $\sigma = E \cdot \varepsilon$  and anelastic deformation  $\varepsilon_a = \varepsilon \cdot \Delta E / E$ . Within the framework of the string model of the elastic region of small deformations, the damping exists because of the hysteresis of motion of dislocation segments and its absolute

value depends on the density of mobile dislocations and the distribution along the lengths of their segments [17]. The dislocation hysteresis of the occurrence of nonlinear damping and softening modulus  $E$  is related to the basic one for metals and its alloys and is described by the breakaway mechanism within the Granato–Lücke theory [17] or by the generalized friction mechanism [18].

## 2. MATERIALS AND METHODS

The materials studied in this work were obtained by casting at SOMZ (Solikamsk Experimental Metallurgical Plant) from a furnace charge mixture of the composition Mg–2.6Y–1Zn–0.5Gd–0.2Zr–0.1Yb based on technically pure components. The resulting castings were subjected to homogenizing annealing at the temperature of 525 °C for 12 hours. Alloys of this composition have an elevated ignition temperature and can be used to manufacture power and body parts of aerospace transport systems [19]. In addition, obtaining high damping properties for the materials used in these industries is a particularly pressing task.

The specimens for the damping studies were cut from the cast ingots using a precision sectioning saw (IsoMet 1000 Buehler) and grounded with P400 grit silicon carbide abrasive discs as shown in Figure 1a. The shape of the specimens corresponded to the rod to ensure standing elastic vibrations in the longitudinal direction [20,21]. The samples intended for microscopic studies and X-ray structural analysis were ground in the  $x$ - $y$  plane (Fig. 1a) with carbide abrasive discs (grit range up to P800) and polished with 1  $\mu$ m water-based diamond suspension. Optical microscopy investigations were performed on samples additionally etched by immersion in a 5% nitric acid solution in isopropyl alcohol for 1 min at room temperature. Comparative analyses of X-ray diffraction patterns of samples before and after grinding into powder with a particle size of less than 100  $\mu$ m was also performed.

Microstructural studies were carried out using SEM—scanning electron microscopy (MIRA III Tescan), optical microscopy (MET-5T Altami) and X-ray powder diffraction (MD-10 Radikon and DRON-8 Bourevestnik JSC). Element analysis of the alloy samples was performed using an energy dispersive microanalysis (Ultim

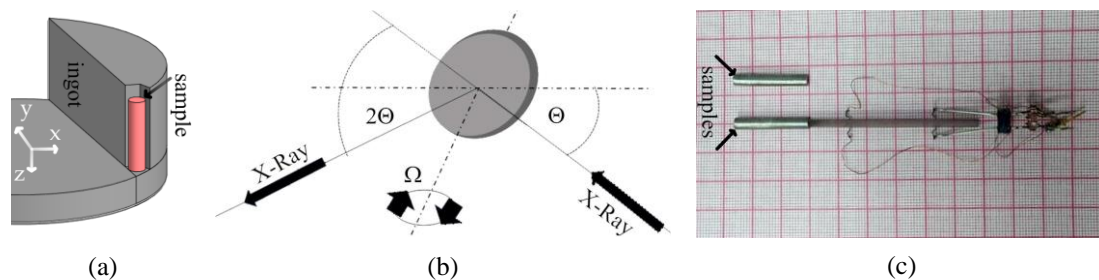


**Fig. 1.** Schematic of sample cutting (a), X-ray diffraction studies (b) and elastic vibration test (c).

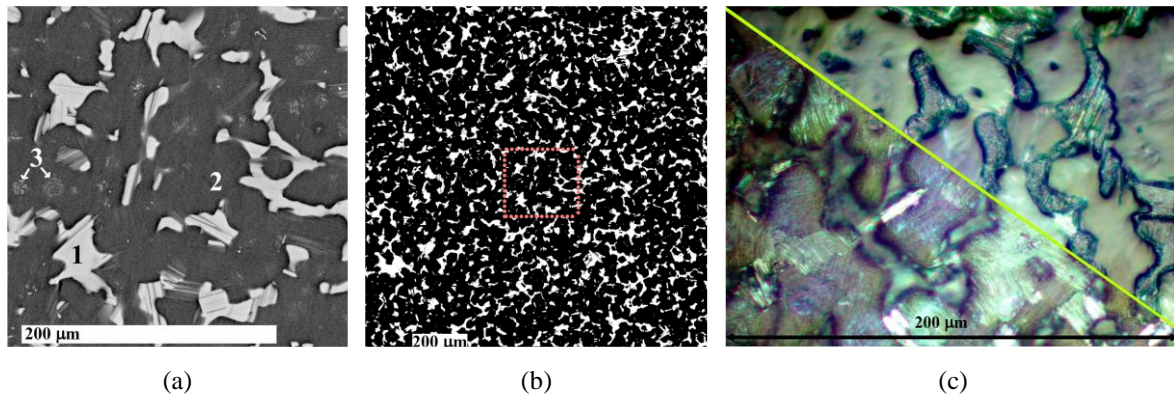


**Fig. 2.** Surface of the investigated magnesium alloy: scanning electron microscopy image in backscattered electron contrast (a), binarized contrast for calculating the area ratio (b), optical microscopy when focusing on different (separated by green line) areas (c).

Max-100 Oxford Instruments) system integrated with SEM. Both the total spectra over the sample area (Fig. 2a) and the spectra at individual points with high Z-contrast were measured. X-ray diffraction (XRD) data of the cast samples were obtained using monochromatized  $\text{CrK}_\alpha$  emission of  $\text{LiF}(200)$  by  $\Omega$ -rotation of the ingots at a rate of  $10 \text{ min}^{-1}$  (Fig. 1b). In addition, the comparison of X-ray diffraction from powder and ingot samples was carried out using  $\text{CuK}_\alpha$  radiation. The full-profile Rietveld analysis using the GSAS software package was applied to refine the phase X-ray diffraction analysis data [22].

The measurements of elastic oscillation damping and effective elastic modulus in the samples were carried out both at room temperature and under liquid nitrogen cooling with oscillatory strain amplitudes in the range from  $10^{-7}$  to  $10^{-4}$  using the piezoelectric resonant composite oscillator method described in detail in Ref. [20]. The sample was attached with cyanoacrylate glue. Longitudinal oscillations were excited at about 100 kHz while the frequency and amplitude of the generated and measured signal were detected (Fig. 1c). Temperature studies were carried out using a measuring insert and cryostreamer, which are described in detail in Ref. [23]. The density of the samples was measured in isopropanol by standard displacement method using a GH-252 (A&D Company) analytical balance with precise temperature control using a V7-78/1 (AKIP) meter.

### 3. RESULTS AND DISCUSSION

Contrasting blocks of two different brightnesses were observed in SEM images (Fig. 2a, areas 1 and 2) obtained in the backscattered electron mode (BSE). Several clusters of segregation were also visible in the obtained image (Fig. 2a, area 3). The dark phase (Fig. 2a, area 2) has the role of a matrix that surrounds all inclusions and, according to the nature of the Z-contrast, includes a minimum amount of heavy (Y and Gd) elements. In areas 1 and 2, textural patterns discontinuous at the block-

subgrain boundary were observed. According to the EDS data, the element content was as follows in area 1:  $\text{Mg}-6.00\text{Y}-6.82\text{Zn}-1.45\text{Gd}-0.08\text{Zr}-0.05\text{Yb}$ ; and in area 2:  $\text{Mg}-1.47\text{Y}-0.42\text{Zn}-0.50\text{Gd}-0.10\text{Zr}-0.11\text{Yb}$ . The atomic ratio in area 1 was close to the  $\text{Mg}_{12}\text{ZnRE}$  ( $\text{RE} = \text{Y, Gd, Yb}$ ) composition known for LPSO structures [21].

The SEM image obtained in BSE contrast for the larger area was used to determine the area ratio of phases 1 and 2 (phase 3 from phase 2 because of the small fraction and complex morphology were not distinguished). The binarized contrast image (Fig. 2b) shows an area ratio of  $R_{12} \approx 0.165$ . Rich surface morphology of phase 1 blocks (Fig. 2a, area 1) showed that the volume fraction of this phase is less than 16%.

Optical microscopy data of the surface of the samples also showed the presence of two main phases, in terms of colors and brightness contrast. A larger area was more susceptible to etching. The corresponding change in morphology was  $\Delta h \sim 3 \mu\text{m}$  by z-focusing of the microscope.

Thus, according to the microscopy data, the samples of the studied alloy consisted of 2 predominant phases (ratio of about 5:1) with different corrosion resistance. The blocks of the first phase separated by the etching pattern (subgrains) had a size of about  $20 \mu\text{m}$ , while the blocks of the second phase had a complex morphology of mesh shape distributed along grain boundaries similar to one described in Ref. [24].

The X-ray diffraction patterns obtained from the cast samples are shown in Figure 3a. The background increase in the far-angle region is typical for the used equipment (1-D detector of MD-10 Radikon). Reflection peaks on the pattern were indicated in hexagonal and cubic lattice within 3 different phases. Taking into account these data and element composition, a search for specific phases from the Powder Diffraction File™ (PDF® ICDD) database and previously published data (see Refs. [3,11,12,25]) was carried out. Full-profile refinement was performed using the Rietveld method (Fig. 3b). The results showed that the texture coefficient of the 0 0 0 2 peak strongly influences

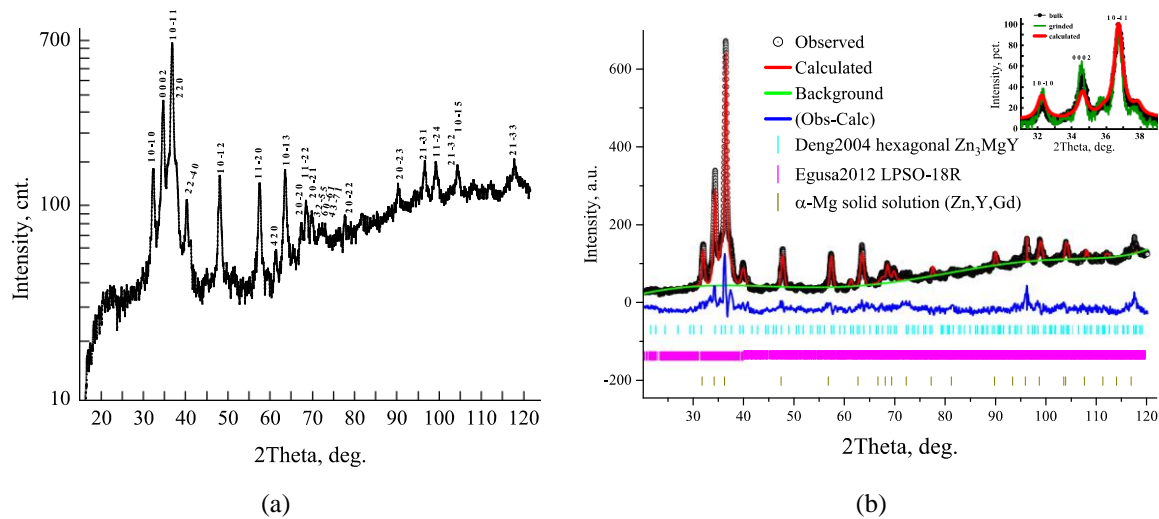


**Fig. 3.** X-ray diffraction pattern (a) and full profile fitting pattern (b) of magnesium alloy, comparison of grinded and bulk material (b, inset).

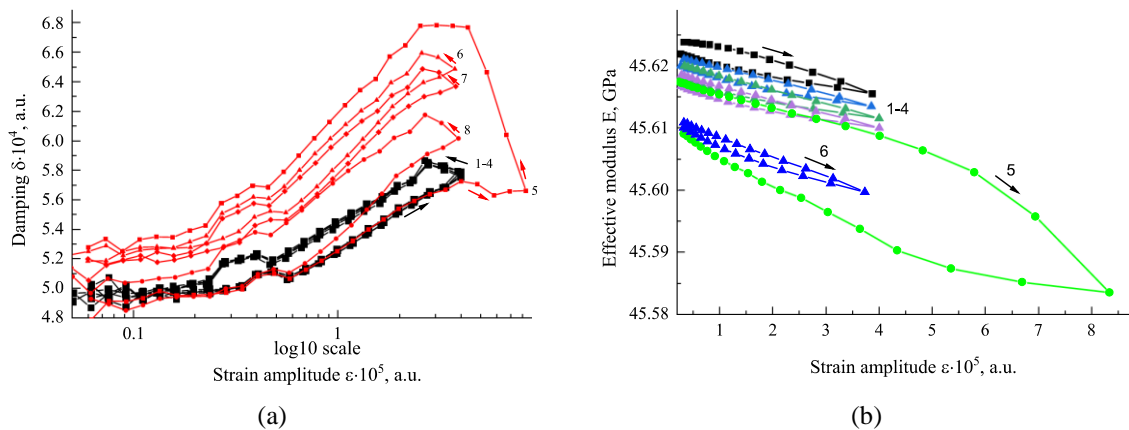


**Fig. 4.** Damping (a) and effective modulus (b) on strain amplitude dependency in the studied magnesium alloy, the numbers indicate the sequence of loading cycles.

the agreement between the calculated and observed diffraction patterns. The ratios of reflectance peaks between  $1\ 0\ \bar{1}\ 0$  and  $0\ 0\ 0\ 2$  as well as  $0\ 0\ 0\ 2$  and  $1\ 0\ \bar{1}\ 1$  in the calculated curve as well as in the PDF 35-821 for  $\alpha$ -magnesium powder show the presence of preferential orientation with ratio of about 0.85 in this hexagonal phase. The weighted mismatch rate  $r_{wp}$  for this case was 0.05 or less. Studies corresponding to the determination of the fraction of the preferentially oriented phase were carried out by obtaining X-ray diffraction in the region of  $2\theta = 30^\circ \div 40^\circ$  from the samples in the form an ingot and powder (Fig. 3b, inset). It should be noted that in this case redistribution of other peaks relative to  $1\ 0\ \bar{1}\ 1$  was observed. Based on the known literature data [21], it was assumed that one of the phases is a nanostructured magnesium 18R LPSO with the composition  $Mg_{12}ZnRE$  and a monoclinic crystal structure. During the refinement, the RE atoms in this phase were occupied according to the EDS data:  $RE = (Y_{0.8}Gd_{0.19}Yb_{0.01})$ . The obtained fraction of the LPSO phase according to XRD analysis was about

10 vol.%. Also, it should be noted that the changes in the intensity of X-ray reflections of  $\alpha$ -Mg could be associated with both the texture observed in individual subgrains by microscopy and uneven distribution of alloying element atoms in the lattice.

The dependences of damping (Fig. 4a) and effective modulus (Figs. 4b) on strain amplitude in the studied magnesium alloy were obtained by the resonant composite oscillator method [20]. Hereinafter, for the data obtained by this method, arrows explain the forward and reverse run in increasing and decreasing strain amplitude, and numbers indicate the sequence of loading cycles. The observed difference between forward and reverse running consisted in the amplitude hysteresis for both values of  $E$  and  $\delta$ . Stable resonant vibrations during measurements occurred in these samples at strain amplitudes  $\varepsilon > 2 \cdot 10^{-7}$ . The damping value was plotted in a logarithmic scale; its linear part was almost absent in the specified range. The character (index) of the logarithmic dependence changed after a certain feature on the curves in the region of  $\varepsilon \sim 3 \cdot 10^{-6}$ . When

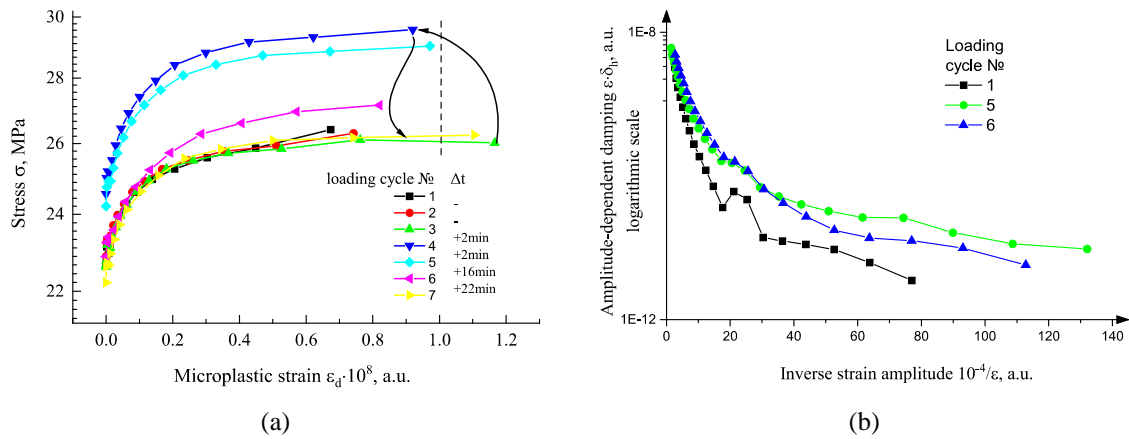


Fig. 5. Stress-strain curves for microplastic deformation (a) and Granato-Lücke plot of damping in the studied magnesium alloy (b).

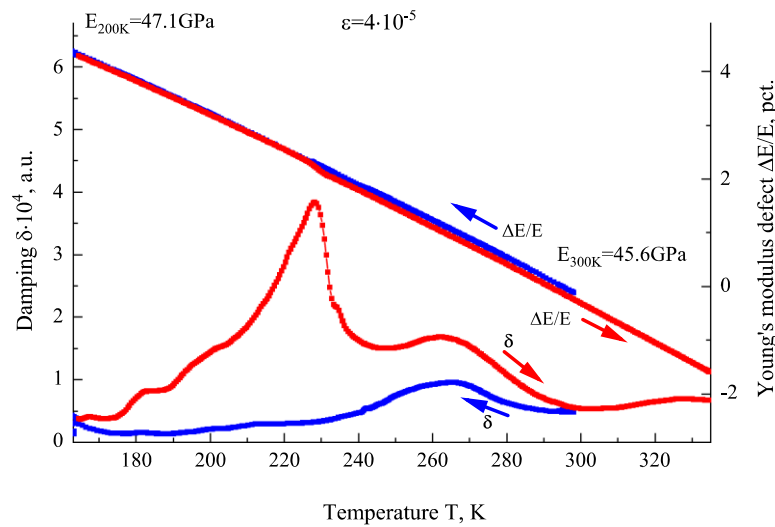


Fig. 6. Temperature dependency of damping and effective modulus changes in the studied magnesium alloy.

the strain amplitude exceeded  $4 \cdot 10^{-5}$ , an increase in the starting damping value was observed, which was inversely dependent on time and fell back to the initial value after about 30 min. An inverse hysteresis of the effective modulus of elasticity  $E$  was observed, with the starting value decreasing with each loading cycle (Figs. 4b). In addition, similar to damping, a sharp softening was observed when the strain exceeded  $4 \cdot 10^{-5}$ . The presence of an amplitude damping peak for metals generally indicates the exhaustion of the low-amplitude anelastic mechanism [15]. As a rule, this mechanism is associated with the redistribution of point defects, their pairs or large groups by dislocations.

The stress-strain curves for some loading cycles are shown in Figure 5a. These curves showed saturation of yield microstresses with relatively low  $\sigma_{\max}$  values (an order of magnitude below the LPSO yield stress [26]) within the studied low-amplitude strain stage. Also, corresponding to the time dependence of the damping hysteresis, the effects lead to an increase in the yielding microstress (Fig. 5a, dashed line). The nonlinear part of the anelastic damping was also presented in the form of a

Granato-Lücke [17] plot (Fig. 5b), which indicated the non-string nature of the nonlinear damping mechanism. A large difference from string mechanism of dislocation damping was observed previously [16] in highly dispersed and anisotropic media (nanostructured materials, composites, etc.).

The temperature dependence of the damping  $\delta$  and softening of the elastic modulus  $\Delta E/E$  in the temperature range from 160 K to room temperature (Fig. 6) was obtained for the forward (cooling) and reverse (heating) run. The changes in the stress relaxation mechanism (elastic oscillations and residual thermoelastic stresses) are indicated by the simultaneous change in both  $\delta$  and  $\Delta E/E$  values at 227 K.

The amplitude dependences of the damping (Fig. 7a) of the elastic modulus (Fig. 7b), similar to the high-temperature curves, were obtained at low temperature  $T = 163 \text{ K}$ . Damping at low temperatures did not stop until the strain amplitude was  $10^{-4}$  (equipment limitation). No dependence on this value on time was observed. The inverse hysteresis of the modulus of elasticity with softening of the

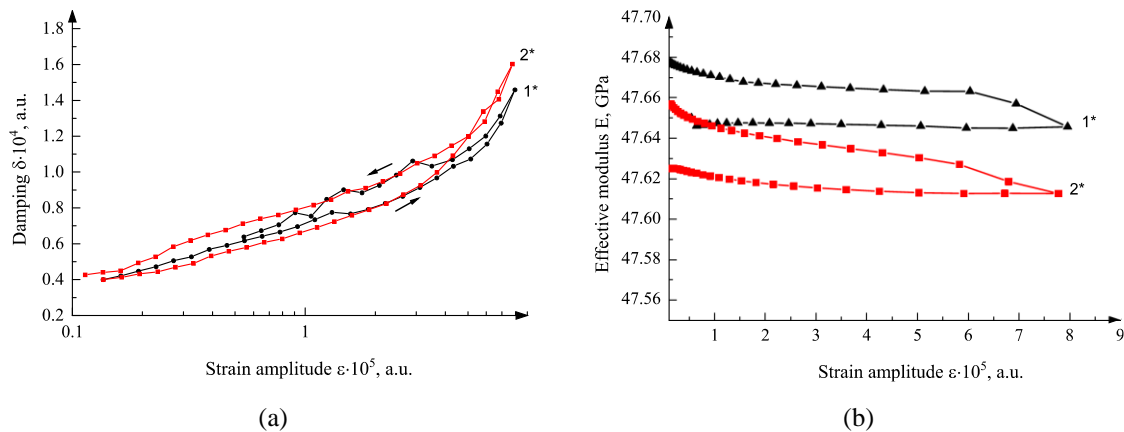


**Fig. 7.** Damping (a) and effective modulus (b) on strain amplitude dependence in the studied magnesium alloy at low temperature  $T = 163$  K.

material in the sequence of loading cycles was preserved (saturation was not investigated).

#### 4. CONCLUSIONS

In this work, magnesium alloys of the Mg-Zn-Y-Gd system obtained by casting and subsequent annealing have been investigated. The characteristics of the samples showed that they are a polycrystalline system of three primary phases: two phases of hexagonal syngony and monoclinic LPSO. The resulting fraction of the 18R LPSO phase according to XRD analysis was about 10 vol.%. In X-ray phase analysis of the samples, effects related to the preferential crystalline orientation and non-uniform distribution of heavy atoms (Y and Gd) introduced into the  $\alpha$ -magnesium lattice were observed. According to microscopic (optical, SEM, and EDS) analysis about 16.5 % of the surface was occupied by LPSO phase with developed morphology.

In the studies by the composite piezoelectric resonator method, growth saturation and maximum damping of elastic oscillations in magnesium alloys were observed. Its appearance indicated the exhaustion of the low-amplitude anelasticity (internal friction) mechanism. The time dependence of the damping was observed when the strain exceeded the amplitude  $4 \cdot 10^{-5}$  and was explained by the redistribution of mobile point defects (or groups of point defects) by dislocations. In the low-temperature studies, the maximum of damping was not observed, and the time dependence of its nonlinear part and the softening of the elastic modulus were almost absent. The maximum of thermoelastic stress relaxation was observed at 227 K and was explained by the activation of the above mechanism, which is related to the mobility of point defects.

The aforementioned results have shown the high importance of further studies of these alloys to establish the mechanisms of anelasticity and microplasticity (microyielding) and their relationship with macroscopic mechanical properties. Further investigations into the nature of

time-dependent nonlinear damping, intra- and interphase grain-boundary interactions, and the conditions of movement and replication of dislocation at these boundaries are needed. The relationship between microplastic and macroscopic properties can be established using acousto-plastic studies [27], as well as using combined tensile strength and acoustic emission tests [28].

#### ACKNOWLEDGMENTS

The authors are grateful to Professors Alexey Romanov, Alexey Vinogradov and Konstantin Sapoghnikov for creating an atmosphere of high-level scientific research and insightful discussions. This study was supported by the Russian Science Foundation, project no. 24-72-00073, <https://rscf.ru/project/24-72-00073/>.

#### REFERENCES

- [1] K.I. Portnoi, A.A. Lebedev, *Magnesium Alloys (Properties and Technology): Handbook*, Metallurgizdat, Moscow, 1952.
- [2] V.A. Duyunova, A.A. Leonov, N.V. Trofimov, A.S. Rostovtseva, Effect of qualitative and quantitative ratios of rare-earth elements in a new fireproof cast magnesium alloy, *Russ. Metall.*, 2021, vol. 2021, no. 11, pp. 1409–1412.
- [3] E.M. Padezhnova, E.V. Mel'nik, R.A. Miliyevskiy, T.V. Dobatkina, V.V. Kinzhbalo, Investigation of the Mg-Zn-Y system, *Russ. Metall.*, 1982, no. 4, pp. 185–188.
- [4] Z. Savaedi, H. Mirzadeh, R. M. Aghdam, R. Mahmudi, Effect of grain size on the mechanical properties and biocorrosion resistance of pure magnesium, *J. Mater. Res. Technol.*, 2022, vol. 19, pp. 3100–3109.
- [5] Y.-X. Luo, B.-X. Dong, H.-Y. Yang, F. Qiu, B.-C. Yan, S.-L. Shu, Q.-C. Jiang, F.-J. Shi Research progress on nanoparticles reinforced magnesium alloys, *J. Mater. Res. Technol.*, 2024, vol. 30, pp. 5166–5191.
- [6] H. Somekawa, Effect of alloying elements on fracture toughness and ductility in magnesium binary alloys; A review, *Mater. Trans.*, 2020, vol. 61, no. 1, pp. 1–13.
- [7] H.E. Friedrich, B.L. Mordike, *Magnesium Technology*, Springer-Verlag, Berlin/Heidelberg, 2006.

- [8] S.-J. Huang, S.-Y. Wu, M. Subramani, Effect of zinc and severe plastic deformation on mechanical properties of AZ61 magnesium alloy, *Materials*, 2024, vol. 17, no. 7, art. no. 1678.
- [9] M. Sun, D. Yang, Y. Zhang, L. Mao, X. Li, S. Pang, Recent Advances in the Grain Refinement Effects of Zr on Mg Alloys: A Review, *Metals*, 2022, vol. 12, no. 8, art. no. 1388.
- [10] Y. Yang, C. Ling, Y. Li, S. Peng, D. Xie, L. Shen, Z. Tian, C. Shuai, Microstructure development and biodegradation behavior of additively manufactured Mg-Zn-Gd alloy with LPSO structure, *J. Mater. Sci. Technol.*, 2023, vol. 144, pp. 1–14.
- [11] E. Oñorbe, G. Garcés, P. Pérez, P. Adeva, Effect of the LPSO volume fraction on the microstructure and mechanical properties of Mg-Y<sub>2x</sub>-Zn<sub>x</sub> alloys, *J. Mater. Sci.*, 2012, vol. 47, no. 2, pp. 1085–1093.
- [12] D. Deng, K. Kuo, Z. Luo, D. Miller, M. Kramer, K. Dennis, Crystal structure of the hexagonal Zn<sub>3</sub>MgY phase, *J. Alloys Compd.*, 2004, vol. 373, no. 1–2, pp. 156–160.
- [13] J. Hao, L. Zhao, J. Zhang, W. Cheng, Effect of unequal channel angular pressing on microstructure and mechanical properties of Mg-Zn-Y-Mn-Ti magnesium alloy enhanced by lamellar LPSO phase and spherical W phase, *J. Mater. Res. Technol.*, 2025, vol. 35, pp. 4204–4216.
- [14] J. Marx, Use of the piezoelectric gauge for internal friction measurements, *Rev. Sci. Instrum.*, 1951, vol. 22, no. 7, pp. 503–509.
- [15] R.H. Chambers, R. Smoluchowski, Time-dependent internal friction in aluminum and magnesium single crystals, *Phys. Rev.*, 1960, vol. 117, no. 3, pp. 725–731.
- [16] K. Sapozhnikov, S. Golyandin, S. Kustov, Elastic and anelastic properties of C/Mg-2wt.%Si composite during thermal cycling, *Compos. Part A Appl. Sci. Manuf.*, 2009, vol. 40, no. 2, pp. 105–113.
- [17] A. Granato, K. Lücke, Theory of mechanical damping due to dislocations, *J. Appl. Phys.*, 1956, vol. 27, no. 6, pp. 583–593.
- [18] S. Asano, Theory of nonlinear damping due to dislocation hysteresis, *J. Phys. Soc. Japan*, 1970, vol. 29, no. 4, pp. 952–963.
- [19] S.V. Zasytkin, D.L. Merson, A.I. Brilevsky, A.I. Irtegov, On selection of advanced compositions of flame resistant magnesium alloys, *Lett. Mater.*, 2023, vol. 13, no. 2, pp. 104–108.
- [20] S. Kustov, S. Golyandin, A. Ichino, G. Gremaud, A new design of automated piezoelectric composite oscillator technique, *Mater. Sci. Eng. A*, 2006, vol. 442, no. 1–2, pp. 532–537.
- [21] W.H. Robinson, A. Edgar, The piezoelectric method of determining mechanical damping at frequencies of 30 to 200 kHz, *IEEE Trans. Sonics Ultrason.*, 1974, vol. 21, no. 2, pp. 98–105.
- [22] B.H. Toby, R.B. Von Dreele, GSAS-II: the genesis of a modern open-source all purpose crystallography software package, *J. Appl. Crystallogr.*, 2013, vol. 46, no. 2, pp. 544–549.
- [23] D.A. Kalganov, V.V. Kaminskii, N.M. Yurchenko, N.M. Silnikov, I.V. Guk, A.I. Mikhailin, A.V. Podshivalov, A.E. Romanov, Dynamical Young's modulus and internal friction in ultra-high molecular weight polyethylene composites, *Rev. Adv. Mater. Technol.*, 2022, vol. 4, no. 1, pp. 14–20.
- [24] X. Wang, M. Li, Y. Huang, Y. Liu, C. Huang, Deformation behavior of LPSO phases with regulated morphology and distribution and their role on dynamic recrystallization in hot-rolled Mg-Gd-Y-Zn-Zr alloy, *J. Mater. Res. Technol.*, 2023, vol. 26, pp. 6121–6134.
- [25] D. Egusa, E. Abe, The structure of long period stacking/order Mg-Zn-RE phases with extended non-stoichiometry ranges, *Acta Mater.*, 2012, vol. 60, no. 1, pp. 166–178.
- [26] K. Hagihara, Z. Li, M. Yamasaki, Y. Kawamura, T. Nakano, Strain-rate dependence of deformation behavior of LPSO-phases, *Mater. Lett.*, 2018, vol. 214, pp. 119–122.
- [27] K. Sapozhnikov, S. Golyandin, S. Kustov, B. Enflo, C.M. Hedberg, L. Kari, Microstructural mechanisms of the acoustoplastic effect in crystals, *AIP Conf. Proc.*, 2008, vol. 1022, pp. 311–314.
- [28] A. Vinogradov, E. Vasilev, A. Brilevsky, D. Merson, K. Kudasheva, Acoustic emission study of the kinetics of kink bands in the LPSO structure, *Lett. Mater.*, 2019, vol. 9, no. 4, pp. 504–508.

УДК 548.4:539.3

## Низкоамплитудное нелинейное затухание и эффективный модуль в сплавах магния, содержащих фазу с длиннопериодной слоистой структурой

Д.А. Калганов<sup>1</sup>, С.А. Филиппов<sup>1,2</sup>, В.В. Каминский<sup>3</sup>, А.Ю. Иванов<sup>3</sup>, С.В. Засыпкин<sup>4</sup>,  
Д.Л. Мерсон<sup>4</sup>, М.В. Дорогов<sup>3</sup>

<sup>1</sup> Лаборатория дифракционных методов исследования реальной структуры кристаллов, Физико-технический институт им. А.Ф. Иоффе РАН, Политехническая ул., 26, Санкт-Петербург, 194021, Россия

<sup>2</sup> Санкт-Петербургский политехнический университет Петра Великого, Политехническая ул., 29, Санкт-Петербург, 195251, Россия

<sup>3</sup> Институт перспективных систем передачи данных, Университет ИТМО, Кронверкский пр., 49, литер А, Санкт-Петербург, 197101, Россия

<sup>4</sup> Научно-исследовательский институт прогрессивных технологий, Тольяттинский государственный университет, Белорусская ул., 14, Тольятти, 445020, Россия

**Аннотация.** В данном исследовании были охарактеризованы микроструктура и фазовый состав магниевых сплавов, полученных методом литья из шихты Mg–2.6Y–1Zn–0.5Gd–0.2Zr–0.1Yb. Установлено содержание в них около 10% фазы LPSO. Низкоамплитудное нелинейное затухание и умягчение модуля упругости исследованы методом составного пьезоэлектрического резонатора. Выявлена временная зависимость упругости и микропластичности, которая объяснена перераспределением точечных дефектов в упругих полях дислокаций. Указанный механизм активируется при 227 К, что подтверждается наличием пика релаксации напряжений на температурной зависимости затухания, а также отсутствием временной зависимости этой величины при низкотемпературной 163 К деформации.

**Ключевые слова:** неэластичность; нелинейное затухание; эффективный модуль; сплавы магния; длиннопериодная слоистая структура